ELSEVIER

International Journal of Mass Spectrometry 185/186/187 (1999) 291–305

International Journal of Mass Spectrometry

A theoretical study of the isomerization and dissociation processes of the HO–C≡O$^+$ ion: interstate crossing in the formation of H–C≡O$^+$ + O

Paul J.A. Ruttink[a], Peter C. Burgers[b], Johan K. Terlouw[c,*]

[a]*Theoretical Chemistry Group, State University of Utrecht, Centrumgebouw Noord, Padualaan 14, 3584 CH Utrecht, The Netherlands*
[b]*Hercules European Research Center BV, P.O. Box 252, 3770 AG Barneveld, The Netherlands*
[c]*Department of Chemistry, McMaster University, 1280 Main Street West, Hamilton, Ontario L8S 4M1, Canada*

Received 1 June 1998; accepted 27 August 1998

Abstract

Low energy HO–C≡O$^+$ ions [$\Delta H_f(298)$ = 142 ± 2 kcal/mol] uniquely dissociate to H–C≡O$^+$ + O. From ab initio molecular orbital calculations a mechanism is proposed which involves a 1,2-hydrogen shift of HO–C≡O$^+$ ($^1A'$) to H–CO_2^+ ($^1A'$) followed by an interstate crossing leading to a transient triplet $^3A''$ state which then dissociates into H–C≡O$^+$ ($^1\Sigma$) + O (^3P). This mechanism provides a satisfactory explanation of the observed kinetic energy release and it also satisfies the energetic constraints imposed by experiment. From calculations performed at different levels of theory, it became clear that both an advanced level of electronic correlation and large basis sets are a prerequisite for a meaningful description of the above reaction. (Int J Mass Spectrom 185/186/187 (1999) 291–305) © 1999 Elsevier Science B.V.

Keywords: HO–C≡O$^+$; H–CO_2^+; Ab initio calculations; Electronic correlation effects; Interstate crossing

1. Introduction

Protonation of carbon dioxide can occur at two different sites. The most favourable site of protonation is at one of the oxygen atoms and this produces HO–C≡O$^+$, the hydroxy formyl cation. This species is thought to play an important role in the formation of interstellar molecules [1]. In fact, HO–C≡O$^+$ is a confirmed interstellar species [2–5] and is an intermediate involved in reactions in interstellar clouds [6, 7]. In the laboratory, the species can be generated in a mass spectrometer, by dissociative ionization of simple aliphatic carboxylic acids or by protonation of CO_2 [8]. As with many protonated molecules, the most favourable decay process of HO–C≡O$^+$ is not deprotonation, but instead, HO–C≡O$^+$ dissociates unimolecularly to H–C≡O$^+$ + ^{3}O [9]. Since in the ground state HO–C≡O$^+$ is a singlet, this reaction must proceed via a singlet to triplet surface crossing [10]. This reaction produces a Gaussian shaped metastable peak with an average kinetic energy release, $\langle T \rangle$, of 2.5 kcal/mol, which, considering the small

* Corresponding author. E-mail: terlouwj@mcmail.cis.mcmaster.ca.

Dedicated to Professor Mike Bowers in recognition of his impressive contributions to the field of mass spectrometry and ion processes.

PII S1387-3806(98)14173-8

number (four) of vibrational degrees of freedom in the products, may indicate that there is a reverse term.

Experimentally, much less is known about the isomeric form H–CO_2^+, the formyloxy cation. This is because this species lies much higher in energy. In fact, very early ab initio calculations [11] seemed to indicate that this structure is not stable with respect to spontaneous rearrangement to HO–C═O^+. However, subsequent calculations indicated that although H–CO_2^+ is about 90 kcal/mol less stable thermodynamically than HO–C═O^+, a significant isomerization barrier of about 30 kcal/mol, might make H–CO_2^+ a kinetically stable and thus a viable species [12]. Although earlier experimental work indicated that the species had only a transitory existence [13], subsequent work showed that H–COO^+ exists in a potential well and has a lifetime sufficiently long to be observed [14]. In these experiments, the H–CO_2^+ ion is made by collisionally induced two-electron detachment (charge reversal) of the H–CO_2^- anion which is generated by proton abstraction of formic acid in a chemical ionization source. It was observed that 10 μs after its formation, the H–CO_2^+ ions had undergone significant, but not complete, isomerization to HO–C═O^+ [12]. In addition, the H–CO_2^+ ions generated by charge reversal were found to dissociate to H–C═O^+ + ^{3}O, with a similar $\langle T \rangle$ value as found for the HO–C═O^+ ions [15]. Subsequent ab initio calculations [16] indicated that the singlet and triplet forms of H–CO_2^+ have similar energies, lying some 108.3 and 105.8 kcal/mol, respectively above singlet HO–C═O^+ (and that the triplet HO–C═O^+ lies about 99.2 kcal/mol above the singlet state). These energies lie close to, but below the lowest lying sets of products, H–C═O^+ + ^{3}O, $\Sigma\Delta H_f$ = 114 kcal/mol [17]. In addition, the energy barrier for isomerization of the singlet and triplet forms lie 133.7 and 171.6 kcal/mol, respectively above singlet HO–C═O^+ and thus both triplet and singlet H–CO_2^+ are predicted to be stable species in the gas phase.

Nevertheless, it is not clear which H–CO_2^+ ion (singlet or triplet) is formed in the charge reversal experiment: for example, if the triplet is formed, the previous calculations predict that it should rapidly dissociate to H–C═O^+ + ^{3}O without any isomerization to triplet HO–C═O^+. Also, the previous calculations only provide a crude possible mechanism for the metastable formation of H–CO_2^+ from singlet HO–C═O^+: first, the HO–C═O^+ ion (relative energy = 0) undergoes a 1,2-hydrogen shift with an energy barrier of 133.7 kcal/mol to produce singlet H–CO_2^+ which then via crossing of the singlet and triplet surfaces forms triplet H–CO_2^+; this species then dissociates to H–C═O^+ + ^{3}O via simple bond cleavage. However, considering the small (2.5 kcal/mol) kinetic energy release and the small number (four) of vibrational degrees of freedom in the products, the calculated barrier for the reverse reaction (20 kcal/mol) is too large; for example, for a comparable reaction, $CH_2OH^+ \rightarrow$ H–C═O^+ + H_2, 60% of the reverse energy appears as kinetic energy [18].

The purpose of the present study is therefore to obtain, by ab initio molecular orbital (MO) calculations, a better description of the isomerization and dissociation processes of HO–C═O^+ and H–COO^+.

2. Preliminary considerations: heat of formation of HO–C═O^+ and energetical constraints

First, we will assess the reported heats of formation, ΔH_f, for HO–C═O^+. Three methods have been used to determine ΔH_f [HO–C═O^+], namely proton affinity (PA) measurements of CO_2 [19–21], appearance energy (AE) measurements on formic acid [22], and ionization energy (IE) measurements of the HO–C═$O^{\cdot}$ radical [23]. The results are compiled in Table 1 and they refer to 298 K.

The most recent results for the PA (298 K) yield an average value for $\Delta H_f(298)$ = 143 ± 2 kcal/mol, see Table 1. The most extensive calculation of the PA (298 K) has been performed at the coupled-cluster single double (triple) [CCSD(T)]/6-311^{++}G(3*df*, 3*pd*)//CCSD(T)/6-311G(3*df*,3*pd*) level of theory, and this, together with temperature corrections, leads to a $\Delta H_f(298)$ of 141.3 kcal/mol [24].

The AE for HO–C═O^+ formed by loss of $H^{\cdot}$ from formic acid, H–C(═O)–OH has been accurately measured by Ruscic et al. [23], see Table 1, but here a barrier for the reverse reaction may lead to a value

Table 1
Heats of formation, ΔH_f(298 K), of HO–C═O^+ (all values in kcal/mol)

Proton affinity of CO_2	PA	ΔH_f
	129.2 ± 0.5[a]	142.8 ± 0.5
	128.5 ± 1[b]	143.5 ± 1
	128.6 ± 2[c]	143.4 ± 2
Ab initio MO calculation	130.7[d]	141.3
Appearance energy (AE)	AE	ΔH_f
H–$COOH^{\cdot+}$–H$^{\cdot}$	282.8 ± 0.1[e]	140.2 ± 0.2
H–$COOD^{\cdot+}$–H$^{\cdot}$	282.8 ± 0.3[e]	140.2 ± 0.3
D–$COOD^{\cdot+}$–D$^{\cdot}$	287.8 ± 0.1[e]	<145.2 ± 0.3
Ionization energy (IE) $HOCO^{\cdot}$	IE	ΔH_f
	195.7 ± 0.3[f]	149.7 ± 1[g]

[a][19].
[b][20].
[c][21].
[d][24].
[e][22].
[f][23].
[g]Using ΔH_f [$HOCO^{\cdot}$] = −46.0 ± 1 kcal/mol [25].

which is too high. Indeed, ab initio calculations show that loss of H$^{\cdot}$ from ionized formic acid has a reverse barrier of 6 kcal/mol [26] and correcting for the experimental AE by this value would lead to ΔH_f[HO–C═O^+] is 134 kcal/mol which is far lower than the value derived from the PA measurements, see Table 1. However, we have provided evidence that the C–H hydrogen atom in H–C(═O)–OH, but not the C–D deuterium atom in D–C(═O)–OH, may tunnel through the barrier [26] and so the measured AE for loss of H$^{\cdot}$ from H–C(═O)–$OH^{\cdot+}$ might well correspond to formation of the ion HO–C═O^+ at threshold.

Ruscic et al. have also measured the AE for loss of D$^{\cdot}$ from D–C(═O)–$OH^{\cdot+}$, and they find that this AE is significantly larger, by 5 kcal/mol, than that for the loss of H$^{\cdot}$ from H–C(═O)–OH. This observation lends strong support for our proposal that the C–H hydrogen atom in H–C(═O)–$OH^{\cdot+}$, but not the D–C hydrogen atom in D–C(═O)–$OH^{\cdot+}$, may tunnel through the barrier and that by consequence the measured AE for H$^{\cdot}$ from H–C(═O)–$OH^{\cdot+}$ corresponds to HO–C═O^+ ions formed at threshold. Thus from the AE measurements we derive a value of 140.2 ± 1 kcal/mol for ΔH_f[HO–C═O^+].

The AE of the radical HO–C═O$^{\cdot}$ has been measured, IE = 8.486 ± 0.012 eV [23]. The ΔH_f of this radical has been assessed from AE measurements of a variety of precursors [25], ΔH_f[HO–C═O$^{\cdot}$] = −46.0 kcal/mol. These values lead to ΔH_f[HO–C═O^+] = 149.7 kcal/mol, far above the values derived by the AE and PA measurements, see Table 1. It has been suggested that this discrepancy may lie in the fact that there is a large geometry change between the neutral and the ion so that the measured IE may not correspond to an adiabatic ionization energy [24]. In addition, the ab initio value for the AE (at the same level of theory as previously noted [24]) is much lower, 8.00 eV and this leads to ΔH_f[HO–C═O^+] = 138.4 kcal/mol. Based on the above we recommend an experimental value for ΔH_f[HO–C═O^+] of 142 ± 2 kcal/mol and this serves as our anchor level (= 0 kcal/mol).

The dissociation of interest, HO–C═O^+ → H–C═O^+ + ^{3}O, is the dissociation of lowest energy requirement and it is the sole spontaneous reaction observed in the metastable time frame. This reaction has a large calculated activation energy, 113 kcal/mol [17]. The experimental activation energy of the metastable process [9] could not be measured, because the metastable peak was too weak, but an upper limit of the activation energy is provided by the following consideration. At higher internal energies, as evidenced by the collision induced dissociation (CID) mass spectrum [14], other processes come into play, most notably the loss of H$^{\cdot}$ to produce $CO_2^{\cdot+}$. This reaction has a calculated activation energy of 134 kcal/mol [17] and since this simple cleavage process is not observed in the metastable time frame, the metastable ions have excess energies smaller than 21 kcal/mol. There is an even less energy demanding reaction, namely dissociation to H^+ + CO_2, a reaction which is not expected to have a reverse activation energy and for which the calculated activation energy is 130 kcal/mol [17]. This reaction is not routinely observed because of severe instrumental discrimination against ions having very low translational energy. However, starting from 10 keV DO–C═O^+ ions

(generated from $CF_3COOD^{\cdot+}$) we were able to detect a D^+ signal of sizable intensity in the CID mass spectrum, whereas it was clearly absent in the spectrum of the metastable ions. Hence, we can lower the maximum excess energy of the metastable ions to 17 kcal/mol and this represents the maximum leverage for our ab initio calculations.

3. Theoretical methods

3.1. General considerations

Our model of the reaction going from HO–C═O^+ ($^1A'$) to H–C═O^+ ($^1\Sigma^+$) + O (^3P) contains the following steps:

$$HO–C{=}O^+(^1A') \rightarrow TS1 \rightarrow H–CO_2^+(^1A') \quad (1)$$

$$H–CO_2^+(^1A') \rightarrow IC \rightarrow H–CO_2^+(^3A', {}^3A'') \quad (2)$$

$$H–CO_2^+(^3A', {}^3A'') \rightarrow TS2 \rightarrow H–C{=}O^+(^1\Sigma^+) + O(^3P) \quad (3)$$

We start on the singlet potential energy surface (PES) with transition state TS1 corresponding to a 1,2-hydrogen shift, connecting HO–C═O^+ and H–CO_2^+ ($^1A'$). Then we encounter the interstate crossing (IC) in reaction (2) leading to H–CO_2^+ in either the $^3A'$ or $^3A''$ state. Finally, the transition state TS2 in reaction (3) connects the triplet H–CO_2^+ and the dissociation products. The dissociation may proceed via either the $^3A'$ or the $^3A''$ state, since these molecular states both connect to ground state O (^3P) + H–C═O^+. In the $^3A'$ state the a'' lone pair orbital on the O atom is *doubly* occupied, whereas in the $^3A''$ state the a'' lone pair orbital is *singly* occupied. Therefore in the latter state the doubly occupied lone pair orbital may be chosen as the one directed towards the charge on the formyl cation. This is an electrostatically favourable situation and so for large separation the ground state will correspond to the $^3A''$ state. However, it appears that for the HCO_2^+ isomer the $^3A'$ state is substantially lower in energy than the $^3A''$ state. Therefore the transition state for the dissociation has to be calculated for both states.

The most difficult part in the determination of the reaction profile is the identification of the interstate crossing of the $^1A'$ state and either the $^3A'$ or the $^3A''$ state [27]. Using the complete active space self-consistent field (CASSCF) model appears to lead to results which strongly depend on the number and selection of the active space MOs. Using the coupled cluster (CC) method gives less ambiguous results, although the choice between open and closed shell starting points for these calculations should both be considered.

In the following the degenerate 1–3 proton shift in HO–C═O^+ will also be considered:

$$HO–C{=}O^+(^1A') \rightarrow TS0 \rightarrow O{=}C–OH^+(^1A') \quad (4)$$

Since HO–C═O^+ and O═CO–H^+ are equivalent, the transition state TS0 will have C_{2v} symmetry.

The CASSCF calculations discussed in Sec. 3.2 were carried out using the program GAMESS (UK) [28]. For all other calculations the GAUSSIAN 94 suite of programs was used [29].

3.2. CASSCF calculations

The various isomers and dissociation limits encountered in this study vary widely in character. Therefore simple methods like HF cannot be expected to yield useful results (except for the proton affinity of CO_2). For instance, it is not immediately clear whether the ground state of the H–CO_2^+ isomer is a singlet or a triplet. This is indicated by the fact that an UHF calculation taking into account the open shell character of this isomer gives rise to a very large spin contamination.

Since it may reasonably be expected that the dissociation proceeds via a H–CO_2^+-type conformation, we started by performing CASSCF/DZP (CASSCF/double zeta plus polarization) [30] calculations on the isomerization reaction (1). All CASSCF calculations were of the CAS(n,n) type with $n = 2$ or 10. For the $^1A'$ state with $n = 2$ the active MOs may be chosen to be either a' or a'' symmetry. For the H–CO_2^+ ($^1A'$) state this choice appears to be essential. Geometry optimizations of this state using both

choices yield the following results: $E = -187.791\ 17$ H for a' active MOs and $E = -187.717\ 56$ H for a'' active MOs. A calculation using only the (core) $(1a'')^2(2a'')^2(9a')^1(10a')^1\ ^1A'$ configuration yields $E = -187.789\ 19$ H, which is almost the same as the CAS(2,2) result using a' active MOs, whereas a calculation with the core $(9a')^2(10a')^2(1a'')^1(2a'')^1\ ^1A'$ configuration yields $E = -187.670\ 34$ H, which is much higher than the corresponding CAS(2,2) result. Therefore we conclude that for the H–CO_2^+ ($^1A'$) state the active space should at least contain two a' MOs. These correspond to in-plane lone pair orbitals on the O atoms. In order to obtain a continuous PES for the reaction the calculations for HO–C≡O^+ and for the TSs have to satisfy the same requirements as for the H–CO_2^+ isomer.

The results are given in Table 2. It is seen that the geometry of TS1 depends strongly on the number of active MOs N_{act}. Consequently the topology of the PES qualitatively changes on increasing N_{act}, as shown in Fig. 1. For $N_{act} = 2$ the only reasonable possibility is reaction (1), with an activation energy of 99.9 kcal/mol and a large difference between the HCO angles of 30.9°. However, with $N_{act} = 10$ we find that TS0 is lower in energy than TS1 and that both transition states have C_{2v} symmetry ($\langle HCO_1 = \langle HCO_2$). Starting from H–$CO_2^+$ we first arrive at TS1. Here the reaction coordinate is symmetric ($\langle HCO_1 + \langle HCO_2 - 2\langle OCO$). After passing TS1 there is a region where the force constant for this normal coordinate becomes positive, whereas the force constant for the symmetry lowering coordinate $\langle HCO_1 - \langle HCO_2$ becomes negative. Consequently the reaction coordinate changes character and the reaction from here on proceeds to form either HO–C≡O^+ or O≡C–OH^+. The activation energy is determined by TS1. Its value is not much different from the case $N_{act} = 2$, but the corresponding TS geometries are widely different.

A problem with the CASSCF calculations is that various choices for the symmetries of the active MOs are possible, and it is not clear whether there is a unique choice which would describe the entire reaction in a balanced manner. Nevertheless, the calculations indicate that both the $^1A'$ and the $^3A'$ states of H–CO_2^+ correspond to local minima with (near) C_{2v} symmetry.

Table 2
CASSCF electronic (E_{elec}) and relative (E_{rel}) energies (hartree) and geometries (Å/deg) involved in the HO–C≡O^+ → H–CO_2^+ isomerization

	E_{elec}	E_{rel}
2 act MOs		
HO–C≡O^+	−187.919 50	0.0
TS0[a]		
TS1	−187.756 38	99.9
H–CO_2^+ ($^1A'$)	−187.791 17	78.0
H–CO_2^+ ($^3A'$)	−187.793 94	76.3
10 act MOs		
HO–C≡O^+	−188.074 85	0.0
TS0	−187.911 83	102.3
TS1	−187.907 85	104.8
H–CO_2^+ ($^1A'$)	−187.931 39	90.0
H–CO_2^+ ($^3A'$)	−187.922 80	95.4

	CH/OH	CO_1	CO_2	$\langle HCO_1/\langle COH$	$\langle HCO_2/\langle OCO$
2 act MOs					
HO–C≡O^+	0.968	1.218	1.112	119.1	175.0
TS0[a]					
TS1	1.201	1.210	1.169	81.7	112.6
H–CO_2^+ ($^1A'$)	1.085	1.261	1.261	123.8	123.8
H–CO_2^+ ($^3A'$)	1.091	1.256	1.256	118.7	118.7
10 act MOs					
HO–C≡O^+	0.969	1.247	1.138	116.6	174.4
TS0	1.248	1.196	1.196	84.0	84.0
TS1	1.142	1.234	1.234	101.3	101.3
H–CO_2^+ ($^1A'$)	1.080	1.279	1.280	136.7	136.8
H–CO_2^+ ($^3A'$)	1.087	1.286	1.286	118.7	118.6

[a]TS0 does not exist for 2 active MOs.

Another problem arising with the CASSCF calculations is that the geometry corresponding to the interstate crossing appears to be very sensitive to the choice of active MOs. For a small number of active MOs it is not clear whether CASSCF calculations using the same number of active MOs for the singlet and the triplet states yield equally accurate energies. For a large active space the energies should be more reliable, but here the interpretation is complicated by the multitude of solutions to the CASSCF orbital optimization, since even if the MO symmetries are fixed the CASSCF MOs are not at all unique.

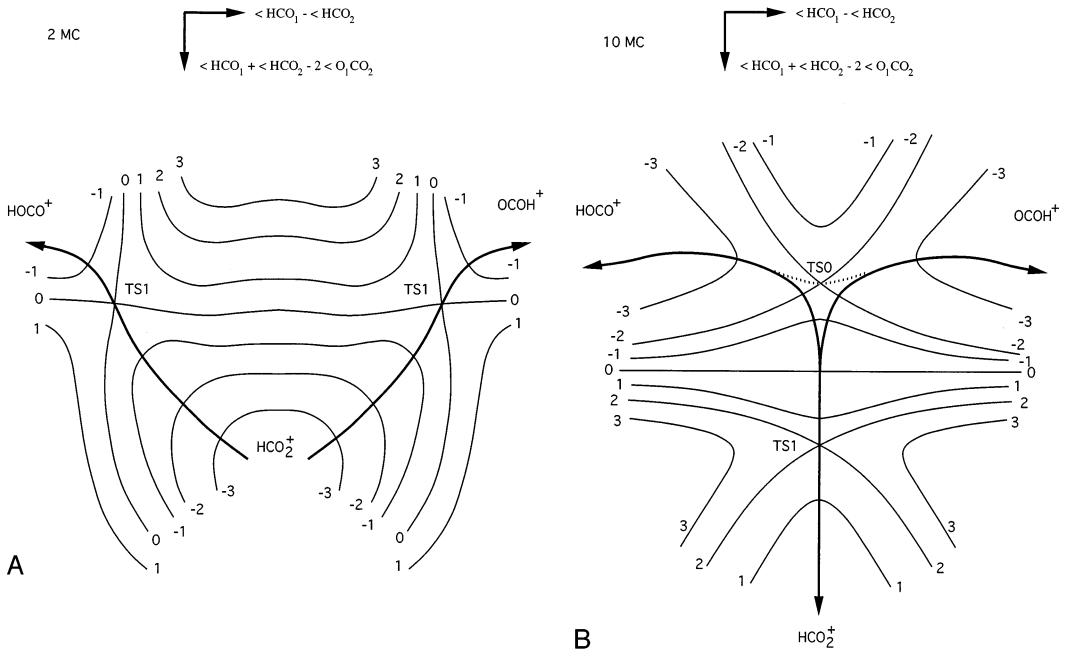

Fig. 1. Schematic contour map of the potential energy surface for the $HOCO^+ \rightarrow HCO_2^+ \rightarrow OCOH^+$ isomerizations as calculated with the CASSCF method. (a) 2 active MOs; (b) 10 active MOs.

3.3. Coupled cluster method

A viable alternative is to choose a single-reference method with inclusion of an advanced level of electronic correlation, such as the coupled cluster method. We have used the CCD(FC)/6-311G(*d*,*p*) [31,32] method for optimizing the geometries. However, here another problem arises, since the UHF method is used for generating the MOs. As is well known, this method may give rise to a large spin contamination, particularly for even electron systems with open shell character (see also abovementioned). Here, too, multiple solutions may exist [33], and for $H–CO_2^+$ we find at least two UHF solutions, one with closed shell character and one with open shell ($\langle S^2 \rangle \approx 1.0$) character.

Even though the open shell UHF solution corresponds to a much lower energy than the restricted Hartree–Fock (RHF) solution, it is not immediately clear which solution should be taken. The unrestricted coupled cluster doubles (UCCD) wave function will still be spin contaminated, leading to an artificial energy lowering, whereas the restricted coupled cluster doubles (RCCD) wave function has the correct spin symmetry, but a comparatively ineffective reference function. Since no information is available about the effect of the UCCD spin contamination on the corresponding energy, it was impossible to decide from our results which approach is the more reliable one. Note that the CC wave functions are nonvariational, so that the corresponding energies have no upper bound property. Note also that a singlet diradical may be represented by either the open shell CSF $\Psi_1 = |a\bar{b}| - |\bar{a}b|$ or by the linear combination of closed shell determinants $\Psi_2 = |c\bar{c}| - |d\bar{d}|$ where a and b are localized (oxygen lone pair) orbitals, whereas c and d are delocalized (a_1 and b_2) linear combinations of a and b.

Therefore both choices were examined and although they do not yield identical results, the final conclusions are not affected by this choice.

Several computational schemes were tried and judged by their capability to reproduce experimentally known relative energies. It appears that it is not

possible to find reliable results if we restrict ourselves to either perturbation theory or to a small atomic orbital (AO) basis set. The Møller–Plesset perturbation theory (MPPT) may well diverge for the singlet state because of the large spin contamination [34]. However, an additivity scheme combining CCSD(T)(FC)/6-311G(d,p) results with MP2(FC)/6-311 + G(3df,2p) [35] results yields satisfactory results for the heats of formation of various dissociation products.

The final energies are thus calculated with

$$E^{el}[\text{final}] = E(\text{6-311G}(d,p))[\text{CCSD(T)}] + E(\text{6-311 + G}(3df,2p))[\text{MP2}] - E(\text{6-311G}(d,p))[\text{MP2}] \quad (5a)$$

$$E[\text{final}] = E^{el}[\text{final}] + 0.95*\text{ZPE}(\text{6-311G}(d,p))[\text{CCD}] \quad (5b)$$

For all stationary points the number of imaginary frequencies was checked and zero-point energy (ZPE) contributions were calculated using CCD/6-311G(d,p) calculations. In order to enable a fair comparison between experimental data and calculated results "experimental" relative electronic energies were derived by subtracting calculated ZPE contributions from 0 K heats of formation. This was done because ZPE contributions for the crossings were not available, since these do not correspond to stationary points on the PESs. The calculated ZPEs were scaled by a factor of 0.95 [36].

4. Results and discussion

4.1. Single reference results

The results of the HF based calculations are given in Tables 3 and 4. The corresponding relative energies are depicted in Figs. 2 and 3. Except for HO–C═O^+, which has clearly closed shell character, all calculations for the $^1A'$ state were carried out in two ways, i.e. by choosing either an open shell or a closed shell startup for the HF calculation by which the MOs, to be used later on, are determined. The differences found are indicated in Figs. 2 and 3 by the shaded areas.

From these results it is clear that the MP2(FC)/6-311G(d,p) method does not yield very useful results. Comparing the MP2 results to the experimental data, we see that the reverse activation energy (RAE) is much too large. Since the geometries calculated with the MP2 method were deemed to be unreliable charged CO, we used CCD(FC)/6-311G(d,p) for optimizing the geometries. Using the additivity scheme explained in the previous subsection the results labeled by "extrap" were obtained. In order to facilitate the comparison with experimental data ΔH_f (298 K) values were corrected to 0 K. "Experimental electronic energy" $E_{\text{el,rel}}$ ("exp") values were then obtained by using calculated ZPE values. The results are given in Table 5. Here we have also applied the higher level correlation correction as used in the G1 method [37] to the calculated energies $E_{\text{el,rel}}$ (calc). This correction shifts the relative H–C═O^+ + O, C–OH^+ + O, and CO + OH^+ levels up by 5.7 mH = 3.6 kcal/mol, thereby decreasing the differences between the experimental and calculated results significantly. The final deviations with respect to all known experimental heats of formation are reasonably small. Also we find a small RAE of approximately 5 kcal/mol which is compatible with the experimental kinetic energy release of 2 kcal/mol for the dissociation.

Some intermediate results are shown in Fig. 3. There is a large difference between the level schemes representing the MP2/6-311G(d,p) and the CCSD(T) results for the same AO basis, indicating the importance of an advanced description of the electronic correlation effects. The MP4 results show that it is difficult to describe these effects properly with perturbation theory. However, although the CCSD(T)/6-311G(d,p) results are clearly an improvement, the agreement with experiment is still rather poor. Including the effects of basis set enhancement on the MP2 level again improves the results substantially, and the final results are in satisfactory agreement with the available experimental data.

Table 3
Electronic (hartree) and relative energies (kcal/mol) for various theoretical methods; for experimental data see the text; the relative energies E_{rel} are calculated using Eq. (5a); the ZPE values are unscaled

	$HOCO^+(^1A')$	$HOCO^+$ (^3A)	HCO_2^+ ($^1A'$)[b]	HCO_2^+ ($^1A'$)[c]	HCO_2^+ ($^3A'$)	
HF	−187.901 76	−187.783 49	−187.805 48	−187.700 29	−187.809 20	
$\langle S^2\rangle$	0.0	2.01	1.03	0.0	2.02	
MP2/small	−188.415 53	−188.226 38	−188.226 60	−188.246 51	−188.231 22	
MP4	−188.442 95	−188.263 78	−188.270 70	−188.285 07	−188.275 36	
CCD	−188.406 50	−188.238 07	−188.248 16	−188.231 78	−188.252 20	
CCSD(T)	−188.434 75	−188.265 01	−188.274 54	−188.274 14	−188.279 43	
ΔMP2[a]	−0.105 87	−0.102 19	−0.100 28	−0.108 08	−0.100 23	
$\boldsymbol{E_{rel}}$	**0.0**	**108.8**	**104.0**	**99.4**	**101.0**	
ZPE	13.9	12.4	12.2	13.0	12.2	
	HCO_2^+($^3A''$)	HCO^+/O (^3P)	COH^+/O (^3P)	CO/OH^+ ($^3\Sigma^+$)	CO_2/H^+	
HF	−187.776 82	−187.802 90	−187.751 74	−187.764 95	−187.685 34	
$\langle S^2\rangle$	2.13	2.0	2.0	2.01	0.0	
MP2/small	−188.193 71	−188.234 17	−188.159 26	−188.188 97	−188.198 55	
MP4	−188.240 09	−188.271 47	−188.203 17	−188.230 32	−188.223 74	
CCD	−188.217 94	−188.245 74	−188.183 34	−188.206 29	−188.184 20	
CCSD(T)	−188.252 04	−188.266 18	−188.201 93	−188.226 72	−188.213 78	
ΔMP2[a]	−0.099 28	−0.092 12	−0.093 70	−0.089 57	−0.113 07	
$\boldsymbol{E_{rel}}$	**118.8**	**114.4**	**153.7**	**140.8**	**134.1**	
ZPE	12.0	10.5	8.6	7.8	7.5	
	TS0 ($^1A'$)[d]	TS1 ($^1A'$)[d]	TS1 ($^1A'$)[b]	TS2 ($^3A''$)	TS2 ($^3A'$)	
HF	−187.715 71	−187.750 77	−187.696 96	−187.764 95	−187.753 78	
$\langle S^2\rangle$	0.0	0.88	0.0	2.26	2.16	
MP2/small	−188.274 51	−188.210 73	−188.266 96	−188.181 92	−188.185 06	
MP4	−188.304 24	−188.256 53	−188.306 09	−188.232 12	−188.231 04	
CCD	−188.246 52	−188.222 30	−188.238 48	−188.205 51	−188.203 96	
CCSD(T)	−188.287 31	−188.278 85	−188.287 20	−188.255 64	−188.237 52	
ΔMP2[a]	−0.109 27	−0.103 67	−0.106 89	−0.097 73	−0.098 20	
$\boldsymbol{E_{rel}}$	**90.4**	**99.2**	**92.0**	**117.5**	**128.6**	
ZPE	9.9	8.7		10.5	10.7	
	IC ($^1A'$)[b]	IC ($^1A'$)[b]	IC ($^1A'$)[c]	IC ($^3A''$)[c]	C ($^3A'$)[e]	C ($^3A''$)[e]
HF	−187.777 25	−187.763 90	−187.653 57	−187.753 22	−187.766 99	−187.766 66
$\langle S^2\rangle$	0.98	2.15	0.0	2.27	2.08	2.22
MP2/small	−188.202 69	−188.190 19	−188.183 93	−188.181 11	−188.193 51	−188.184 94
MP4	−188.248 70	−188.238 50	−188.245 49	−188.232 25	−188.241 47	−188.233 03
CCD	−188.223 71	−188.212 18	−188.177 72	−188.201 75	−188.215 08	−188.207 44
CCSD(T)	−188.256 20	−188.257 80	−188.246 22	−188.252 17	−188.248 19	−188.248 24
ΔMP2[a]	−0.101 46	−0.099 59	−0.103 53	−0.098 23	−0.099 82	−0.096 65
$\boldsymbol{E_{rel}}$	**114.8**	**115.0**	**119.8**	**119.4**	**120.9**	**122.8**

[a]Small: 6-311G(*d*,*p*) AO basis set, large: 6-311+G(3*df*,2*p*) AO basis set.
[b]Geometry calculated with open shell UHF startup.
[c]Geometry calculated with closed shell RHF startup.
[d]In both calculations the geometry from the open shell UHF startup was used. Attempts to locate this TS using RHF were unsuccessful.
[e]Crossing between the $^3A'$ and $^3A''$ states.

Table 4
CCD/6-311G(*d*,*p*) optimized geometries for the stationary points; for the crossings (IC and C) extrapolated energies [Eq. (5a), see the text] were used

	$HOCO^+$ ($^1A'$)	$HOCO^+$ (^3A)[a]	HCO_2^+ ($^1A'$)[b]	HCO_2^+ ($^1A'$)[b]	HCO_2^+ ($^3A'$)
CH/OH	0.980	0.981	1.107	1.092	1.113
CO_1	1.228	1.234	1.261	1.255	1.256
CO_2	1.118	1.297	1.261	1.255	1.256
$\langle HCO_1/\langle COH$	117.0	117.3	118.0	138.9	117.5
$\langle HCO_2/\langle OCO$	174.7	119.6	118.0	138.9	117.0
	HCO_2^+ ($^3A''$)	TS0 ($^1A'$)[b]	TS1 ($^1A'$)[b]	TS2 ($^3A'$)	TS2 ($^3A''$)
CH/OH	1.100	1.275	1.237	1.105	1.094
CO_1	1.324	1.176	1.221	1.128	1.187
CO_2	1.237	1.176	1.176	1.627	1.399
$\langle HCO_1/\langle COH$	126.0	82.3	84.1	146.4	136.2
$\langle HCO_2/\langle OCO$	120.1	82.3	112.3	114.0	119.2
	IC[b]	IC[c]	C ($^3A'/^3A''$)[d]		
CH/OH	1.09	1.09	1.082		
CO_1	1.21	1.20	1.174		
CO_2	1.37	1.50	1.497		
$\langle HCO_1/\langle COH$	138	140	138		
$\langle HCO_2/\langle OCO$	122	126	111		

[a] $\langle HCOH = 165.9$, this state is not planar.
[b] Open shell (U)HF startup.
[c] Closed shell (R)HF startup.
[d] Crossing.

We have also compared various levels of coupled cluster calculations (Fig. 3). This shows the importance of the single and triple excitations. The most conspicuous feature of the CCD level scheme is that this method is clearly incapable of representing the interstate crossing reasonably well. Comparison of the CCD, CCSD, and CCSD(T) results shows that the single excitations reduce the inaccuracies, but the triple excitations turn out to be especially important.

4.2. Effect of open shell character for the $^1A'$ state

The two choices, i.e. open shell or closed shell startup for the HF calculations, sometimes give rise to widely different results for either MP2, MP4, or CCD calculations [38]. Fig. 3 shows that the differences between the results for the open and closed shell startups tend to disappear only if the triple excitations are included in the CC method. In the extrapolated results the differences are again somewhat larger because of the sensitivity of the MP2 energies to these effects (see Fig. 2). Since no analytical gradients were available for the CCSD(T) method all geometry optimizations were performed using CCD, with the 6-311G(*d*,*p*) basis set.

For the transition state TS0 we find a closed shell solution only. This agrees with the CASSCF active MO occupations for this TS, which do not differ much from the closed shell reference determinant values (either 2 or 0). For TS1 we find an open shell-type solution with a geometry similar to the TS1 geometry for the CASSCF ($N_{act} = 2$) calculation. The CCD calculations thus suggest that there is a transition state separating HO–C≡O^+ ($^1A'$) and H–CO_2^+ ($^1A_1$) with $\langle HCO_1 \approx 84°$ and $\langle HCO_2 \approx 112°$ (see Table 4). However, a CCD calculation with closed shell startup for this geometry yields a significantly lower energy. Moreover, if we apply the basis set extension correction as explained in Sec. 4.1, we find that the final

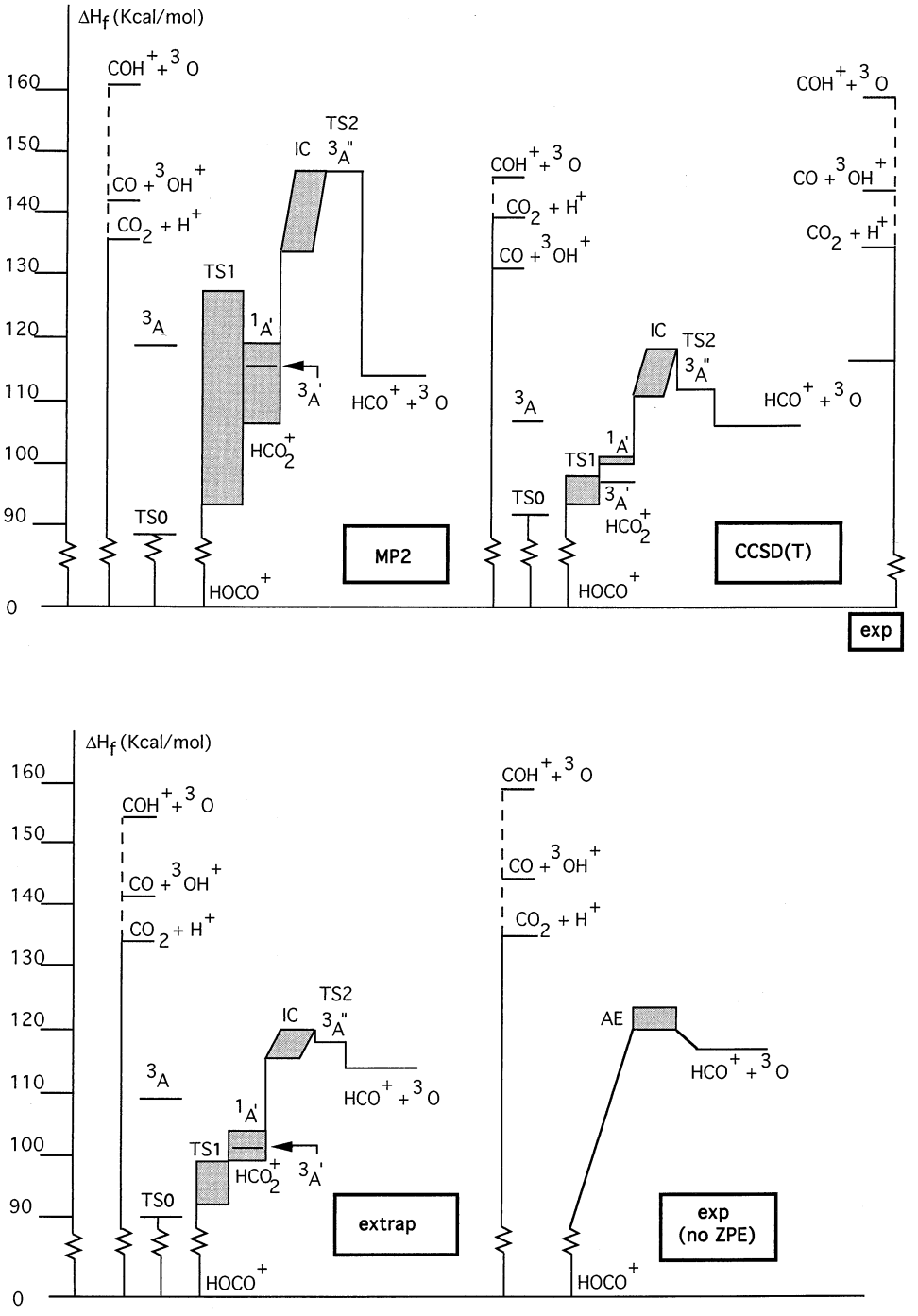

Fig. 2. Comparison of relative electronic energies in kcal/mol for various theoretical methods and experiment. The ZPE contributions are subtracted from the experimental data in order to enable the comparison to electronic energies.

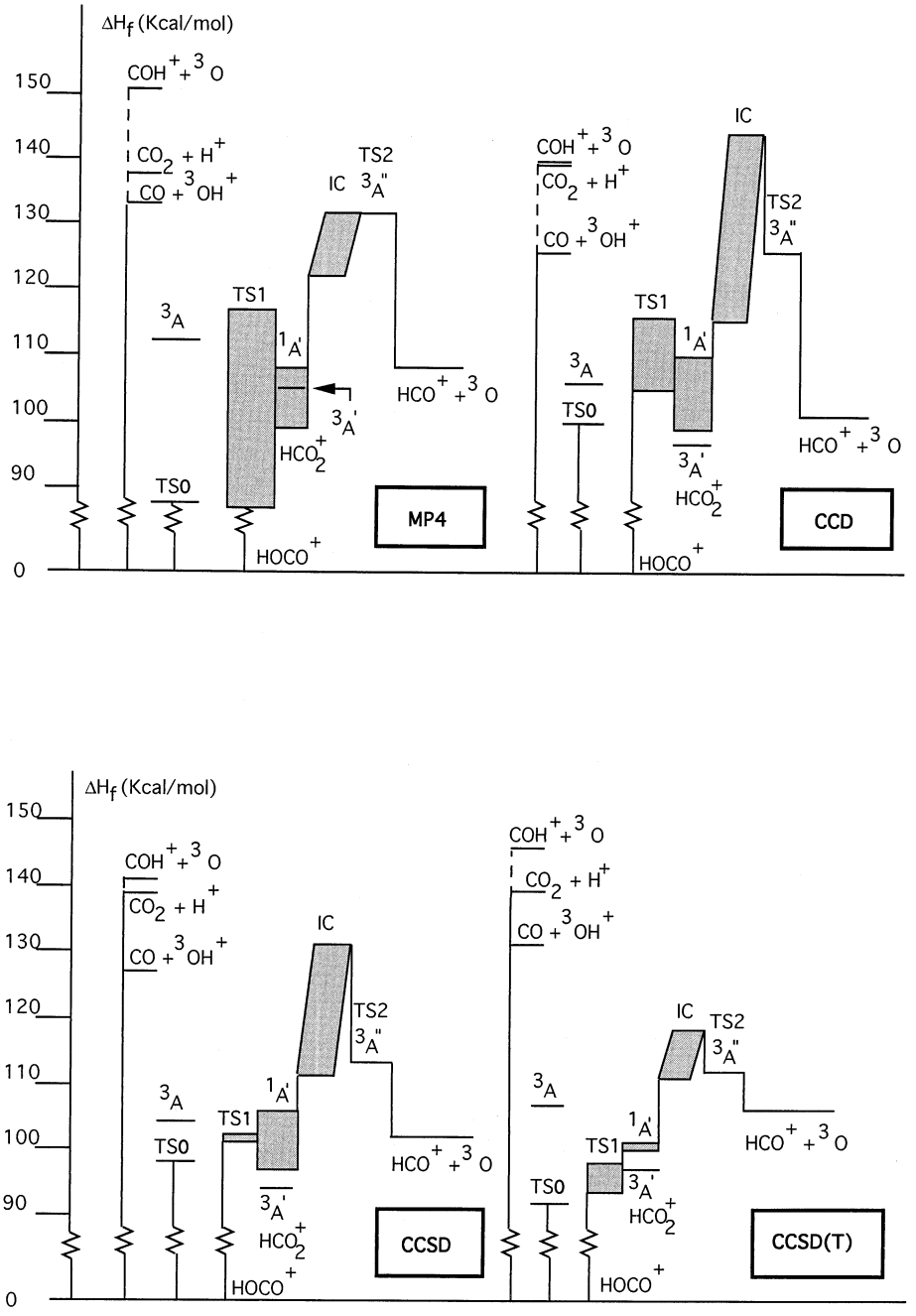

Fig. 3. Effects of single and triple excitations on the relative energies.

energy for this geometry is substantially lower than the H–CO_2^+ ($^1A_1$) final energy. Therefore we conclude that this transition state is an artefact.

Using symmetry-broken localized orbitals in the open shell startup, we also find a stationary point with a geometry close to the CASSCF (N_{act} = 10) result

Table 5
Experimental data [17] used to calculate "experimental electronic energies" $E_{el,rel}$ ("exp"); HLC is the higher level correlation correction according to the G1 model and $E_{el,rel}$ (calc) is obtained from the calculated E_{rel} (extrap) (Table 3) by including the HLC; all energies are in kcal/mol

Species	ΔH_f (298 K)	$\Delta H_{f,rel}$ (0 K)	ZPE (scaled)	E_{rel} ("exp")	HLC	E_{rel} (calc)
HO–C≡O^+	142.0	0.0	13.2	**0.0**	0.0	0.0
HCO^+ + O	256.9	114.5	10.0	**117.7**	3.6	118.0
HOC^+ + O	297.2	154.0	8.2	**159.0**	3.6	157.3
CO_2 + H^+	271.7	129.2	7.1	**135.3**	0.0	134.1
CO + OH^+	282.7	139.8	7.4	**145.6**	3.6	144.4

with C_{2v} symmetry. However, this geometry appears to correspond to a second order saddle point (two imaginary frequencies, corresponding to both normal modes involving the valence angles, viz. ⟨HCO_1 + ⟨HCO_2 − 2 ⟨OCO and ⟨HCO_1 − ⟨HCO_2).

The closed shell startup does not work here because two doubly occupied MOs of different symmetry (a_1 and b_2) cross in the neighbourhood of this geometry, resulting in a crossing between the restricted Hartree–Fock (RHF) potential energy surfaces corresponding to $\Psi_1 \sim$ (core) $(5a_1)^2(1a_2)^2(1b_1)^2(4b_2)^2$ and $\Psi_2 \sim$ (core) $(5a_1)^2(6a_1)^2(1a_2)^2(1b_1)^2$ with (core) = $(1a_1)^2(2a_1)^2(3a_1)^2(4a_1)^2(1b_2)^2(2b_2)^2(3b_2)^2$. This crossing persists in the CCD results, even if the symmetry is lowered to C_s, where the a_1 and b_2 MOs both have a' symmetry. In order to test the performance of the CCSD(T) method for points within the intersection of the PESs corresponding to these occupations, CCSD(T) calculations were performed for a representative point: CH = 1.189, CO_1 = 1.196, CO_2 = 1.234, ⟨HCO_1 = 113.9° ⟨HCO_2 = 122.7°. The results are as follows. HF: −187.59294, −187.59206, CCSD: −188.19312, −188.188 88, CCSD(T): −188.618 41, −188.252 71 for Ψ_1 and Ψ_2, respectively. For Ψ_1 the contribution from the triples appears to be unreasonably large. Therefore accurate results for a rigorously spin adapted coupled cluster type function can only be expected with a multiconfiguration reference function, e.g. with a MR-CCSD calculation, for which, however, no generally applicable implementation was available. In practice, the CASSCF results are thus probably the more significant ones. However, dynamical correlation, here defined as the extra correlation obtained by a CAS-SDCI calculation on top of the CASSCF correlation, may also affect the results. In order to test the importance of this type of correlation CAS-SDCI calculations were performed with four active MOs. The results are as follows. CASSCF: E_1(TS1) = −187.792 62, $E_2(CHO_2^+)$ = −187.818 04, CAS-SDCI: E_1 = −188.009 21, E_2 = −188.013 63, CI + Pople: E_1 = −188.027 33, E_2 = −188.027 30. Here "CI + Pople" indicates the energy obtained by including the size-consistency correction due to Pople, generalized to multiconfiguration reference functions (Ψ_0 is defined as the projection of Ψ_{CI} to the reference space) [40]. From these results it follows that the dynamical correlation substantially lowers the activation energy for the isomerization H–CO_2^+($^1A'$) → HO–C≡O^+ ($^1A'$).

We conclude that it is unlikely that H–CO_2^+ exists as a singlet, although it is difficult to draw a definite conclusion about its stability. Thus the stable H–CO_2^+ ions formed in the charge reversal experiments [14] most likely have the triplet structure whereas the observed rearrangement to HO–C≡O^+ takes place from the singlet HCO_2^+ ion.

4.3. Symmetry of H–CO_2^+

For H–CO_2^+ we find (local) minima for three states: $^1A'$, $^3A'$, and $^3A''$. In the UHF based models the final energies for the $^1A'$ state as calculated with open and closed shell startups bracket the $^3A'$ energy. However, as explained previously, the singlet state may be unstable. The $^3A'$ state, on the other hand, will be stable, since both HO–C≡O^+ (^3A, not planar) and H–C≡O^+ + O (^3P) have much higher energies. In

the leading determinant of the $^3A'$ wave function the a'' lone pair orbitals on the O atoms are doubly occupied.

The determinant with both π lone pair orbitals singly occupied has a much higher energy. In the $^3A''$ state one lone pair AO is doubly occupied, whereas the other one is singly occupied. In agreement with the previous discussion, it lies above the $^3A'$ state for all geometries between HO–C═O$^+$ and H–CO$_2^+$. Therefore in the charge reversal experiments [14] the observed stable triplet H–CO$_2^+$ ions are probably in the $^3A'$ state.

4.4. Symmetry of TS2

For the dissociation step (reaction 3) both $^3A'$ and $^3A''$ states are feasible. The transition states for both were determined and although the CCD energies are nearly the same, the geometries and the basis set enhancement effects are quite different, leading to a substantially lower energy for the $^3A''$ state and a substantially larger CO distance (reaction coordinate) for the $^3A'$ state. This result indicates that the TS energy is determined mainly by the long range electrostatic effect described in Sec. 4.3.

4.5. The interstate crossing

The triple excitations are also crucial for determining the location of the interstate crossing. Since no analytical gradients were available for the CCSD(T) method, the location of the crossing had to be determined by trial and error. Since even for the CCSD(T) method the results for either closed or open shell startups are slightly different in the neighbourhood of the crossing geometry, both choices were considered. One of these nearly coincides with TS2, the other has a somewhat larger CO distance. The energies for the $^3A''$ state for these geometries differ by 4 kcal/mol. In both cases the $^3A'$ state lies above the $^3A''$ state.

Averaging these results we find a geometry near the TS2 geometry. Here the extrapolated energies of the $^1A'$ and the $^3A''$ states are almost equal to each other and to the energy obtained for the $^3A''$ transition state TS2 connecting HCO$_2^+$ and the dissociation products H–C═O$^+$ + O (^3P). The energy requirement for the whole reaction is thus determined by both this transition state and the interstate crossing. Whether the transition state is more important than the crossing in determining the reaction rate cannot be decided from our calculations since it is difficult to find a geometry for which the $^1A'$ and the $^3A''$ states are (nearly) degenerate and also significantly lower in energy than TS2. Such a search is complicated by the difference in results for the $^1A'$ state corresponding to either closed or open shell startups.

4.6. Crossing between the $^3A'$ and $^3A''$ states

In order to assess the importance of the $^3A''$ state we also calculated the minimum energy crossing point (MECP) for the $^3A'/^3A''$ crossing [40]. Since these states may be expected to have correlation energies of comparable magnitude, this was done at the RHF/DZP level.

The final results indicate that this crossing is energetically accessible. However, if we take the longer CO distance as the reaction coordinate for the dissociation, we see that we first encounter the $^3A''$ transition state TS2 which (almost) coincides with the $^1A'/^3A''$ crossing. After this we arrive at the $^3A'/^3A''$ crossing. However, for this CO distance the $^3A''$ state formed near the TS2 ($^3A''$) geometry will in fact have a lower energy. Thus the $^3A'$ state is too high in energy for playing an important role in the dissociation step.

5. Conclusions

In this article we have modeled the metastable reaction HO–C═O$^+$ ($^1A'$) → H–C═O$^+$ ($^1\Sigma^+$) + O (^3P) using high level ab initio MO calculations. In agreement with experiment we find that loss of O (^3P) is the least energy demanding reaction and that it should be the sole reaction, as observed. The reaction commences with a 1,2-hydrogen shift to produce H–CO$_2^+$ in the singlet state which undergoes an interstate crossing to produce a transient triplet ($^3A''$) state, which then dissociates. The reverse reaction

energy (2.5 kcal/mol) originates from the interstate crossing and/or from the barrier to dissociation for the $^3A''$ state. The calculations show that only one configuration of H–CO_2^+ is stable, namely the $^3A'$ state. The singlet ($^1A'$) state is probably unstable towards isomerization into singlet $HOCO^+$, whereas the triplet ($^3A''$) state dissociates to H–C═O^+ + O (^3P). Previously reported charge reversal experiments can be rationalized on the basis of these findings: the experiments may well produce a mixture of H–CO_2^+ in the different states. The $^1A'$ state isomerizes to HO–C═O^+ ($^1A'$), the $^3A''$ state dissociates to H–C═O^+ + O (^3P), whereas the $^3A'$ state remains unchanged.

Acknowledgements

One of the authors (P.J.A.R.) thanks the Netherlands Organization for Scientific Research (NWO) for making available computer time at SARA (Amsterdam) through the Netherlands Foundation for Chemical Research (SON). He also thanks Dr. H. Rudolph for stimulating discussions and for making available computer facilities. Another author (J.K.T.) thanks the Natural Sciences and Engineering Research Council of Canada (NSERC) for financial support.

References

[1] E. Herbst, W. Klemperer, Astrophys. J. 185 (1973) 505.
[2] P. Thaddeus, M. Guelin, R.A. Linke, Astrophys. J. 246 (1981) L41.
[3] M. Bogey, C. Demuynek, J.L. Destombes, J. Chem. Phys. 84 (1986) 10.
[4] T. Amano, K. Tanaka, J. Chem. Phys. 83 (1985) 3721.
[5] D.A. Williams, Chem. Eur. 3 (1997) 1929.
[6] M.J. Frost, P. Sharkey, I.W.M. Smith, Faraday Discuss. Chem. Soc. 91 (1991) 305.
[7] R.S. Berry, Annu. Rev. Phys. Chem. 22 (1971) 47.
[8] F.W. McLafferty, F. Turecek, Interpretation of Mass Spectra, 4th ed., University Science Books, Mill Valley, CA, 1993.
[9] P.C. Burgers, J.L. Holmes, A.A. Mommers, Int. J. Mass Spectrom. Ion Processes 54 (1983) 283.
[10] F. Remacle, S. Petitjean, D. Deharing, J.C. Lorquet, Int. J. Mass Spectrom. Ion Processes 77 (1987) 187.
[11] S. Green, H. Schor, P.E. Siegbahn, P. Thaddeus, Chem. Phys. 17 (1976) 479.
[12] U. Seeger, R. Seeger, J.A. Pople, P. Von R. Schleyer, Chem. Phys. Lett. 55 (1978) 399.
[13] M.M. Bursey, D.J. Harvan, C.E. Parker, L.G. Pedersen, J.R. Hass, J. Am. Chem. Soc. 101 (1979) 283.
[14] P.C. Burgers, J.L. Holmes, J.E. Szulejko, Int. J. Mass Spectrom. Ion Processes 57 (1984) 159.
[15] P.C. Burgers, unpublished results.
[16] (a) J.G. Lu, X.Y. Fu, R.Z. Liu, K. Yamashita, N. Koga, K. Morokuma, Chem. Phys. Lett. 125 (1986) 438; (b) for a very recent combined experimental and theoretical study of the $[C,H,O_2]^{-/+}$ system, see C.A. Schalley, G. Hornung, D. Schröder, H. Schwarz, Int. J. Mass Spectrom. Ion Processes 172 (1998) 181.
[17] (a) S. Lias, J.E. Bartmess, J.F. Liebman, J.L. Holmes, R.D. Levin, W.G. Mallard, J. Phys. Chem. Ref. Data 17 (1988) Suppl. 1; (b) C.G. Freeman, J.S. Knight, J. Glove, M.J. McEwan, Int. J. Mass Spectrom. Ion Processes 80 (1987) 255.
[18] J.H.O.J. Wijenberg, J.H. van Lenthe, P.J.A. Ruttink, J.L. Holmes, P.C. Burgers, Int. J. Mass Spectrom. Ion Processes 77 (1987) 141.
[19] B. Ruscic, M. Schwarz, J. Berkowitz, J. Chem. Phys. 91 (1989) 6772.
[20] N.G. Adams, D. Smith, M. Tichy, G. Javahery, N.D. Twiddy, E.E. Ferguson, J. Chem. Phys. 91 (1989) 4037.
[21] D.K. Bohme, G.I. Mackey, H.I. Schiff, J. Chem. Phys. 73 (1980) 4976.
[22] B. Ruscic, M. Schwarz, J. Berkowitz, J. Chem. Phys. 91 (1989) 11.
[23] B. Ruscic, M. Schwarz, J. Berkowitz, J. Chem. Phys. 91 (1989) 6780.
[24] J.S. Francisco, J. Chem. Phys. 107 (1997) 9039.
[25] J.L. Holmes, F.P. Lossing, P.M. Mayer, J. Am. Chem. Soc. 113 (1991) 9723.
[26] P.J.A. Ruttink, P.C. Burgers, Int. J. Mass Spectrom. Ion Processes 113 (1992) 23.
[27] D.R. Yarkony, in Modern Electronic Structure Theory, D.R. Yarkony (Ed.), World Scientific, Singapore, 1995, Part I, Chap. 11.
[28] M.F. Guest, J. Kendrick. GAMESS (UK) Users Manual, SERC Daresbury Laboratory, CCP/86/1, 1986; M. Dupuis, D. Spangler, J. Wendolowski, NRCC Software Catalog, Vol. 1, Program No. QG01 (GAMESS), 1980; M.F. Guest, R.J. Harrison, J.H. van Lenthe, L.C.H. van Corler, Theor. Chim. Acta 71 (1987) 117.
[29] GAUSSIAN 94, revision E.2 M.J. Frisch, G.W. Trucks, H.B. Schlegel, P.M.W. Gill, B.G. Johnson, M.A. Robb, J.R. Cheeseman, T.A. Keith, G.A. Peterson, J.A. Montgomery, K. Raghavachari, M.A. Al-Laham, V.G. Zakrevski, J.V. Ortiz, J.B. Foresman, C.Y. Peng, P.Y. Ayala, W. Chen, M.W. Wong, J.L. Andres, E.S. Replogle, R.L. Martin, D.J. Fox, J.S. Binkley, D.J. de Frees, J. Baker, J.P. Stewart, M. Head-Gordon, C. Gonzales, J.A. Pople, Gaussian Inc., Pittsburgh, PA, 1995.
[30] (a) T.H. Dunning Jr., J. Chem. Phys. 53 (1970) 2823; (b) T.H. Dunning Jr., P.J. Hay, in Modern Theoretical Chemistry, H.F. Schaeffer III (Ed.), Plenum, New York, 1977, Vol. 3, Methods of Electronic Structure Theory, pp. 1–28.

[31] (a) J. Cizek, Adv. Chem. Phys. 14 (1969) 35; (b) R.J. Bartlett, G.D. Purvis, Int. J. Quantum Chem. 14 (1978) 516.
[32] R. Krishnan, J.S. Binkley, R. Seeger, J.A. Pople, J. Chem. Phys. 72 (1980) 650.
[33] J. Bartlett, H. Sekino, G.D. Purvis III, Chem. Phys. Lett. 98 (1983) 66.
[34] (a) N.C. Handy, P.J. Knowles, K. Somasundram, Theor. Chim. Acta 68 (1985) 87; (b) R.H. Nobes, J.A. Pople, L. Radom, N.C. Handy, P.J. Knowles, Chem. Phys. Lett. 138 (1987) 481.
[35] L.A. Curtiss, C. Jones, G.W. Trucks, K. Raghavachari, J.A. Pople, J. Chem. Phys. 93 (1990) 2537.
[36] A.P. Scott, L. Radom, J. Phys. Chem. 100 (1996) 16502.
[37] (a) J.A. Pople, M. Head-Gordon, D.J. Fox, K. Raghavachari, L.A. Curtiss, J. Chem. Phys. 90 (1989) 5622; (b) L.A. Curtiss, K. Raghavachari, G.W. Trucks, J.A. Pople, ibid. 94 (1991) 7221.
[38] M.J. Frisch, H.F. Schaefer III, J.S. Binkley, J. Phys. Chem. 89 (1985) 2192.
[39] P.J.A. Ruttink, in The Structure of Small Molecules and Ions, R. Naaman, Z. Vager (Eds.), Plenum, New York, 1989, p. 243.
[40] P.J.A. Ruttink, P.C. Burgers, Org. Mass Spectrom. 28 (1993) 1087.